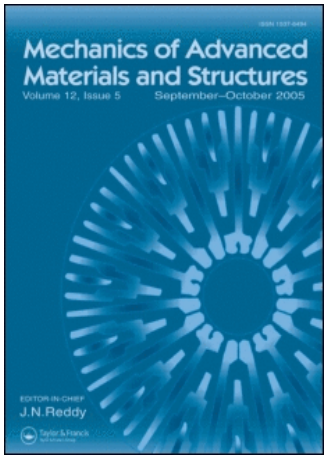

Mechanics of Advanced Materials and Structures
Publication details, including instructions for authors and subscription information:
http://www.informaworld.com/smpp/title~content=t713773278

Analysis of Functionally Graded Plates by a Robust Meshless Method

A. J. M. Ferreira [a]; C. M. C. Roque [a]; R. M. N. Jorge [a]; G. E. Fasshauer [b]; R. C. Batra [c]
[a] Universidade do Porto, Portugal
[b] Illinois Institute of Technology, Chicago, IL, USA
[c] Virginia Polytechnic Institute and State University, Blacksburg, VA, USA

Online Publication Date: 01 November 2007
To cite this Article: Ferreira, A. J. M., Roque, C. M. C., Jorge, R. M. N., Fasshauer, G. E. and Batra, R. C. (2007) 'Analysis of Functionally Graded Plates by a Robust Meshless Method', Mechanics of Advanced Materials and Structures, 14:8, 577 - 587
To link to this article: DOI: 10.1080/15376490701672732
URL: http://dx.doi.org/10.1080/15376490701672732

Mechanics of Advanced Materials and Structures, 14:577–587, 2007

ISSN: 1537-6494 print / 1537-6532 online
DOI: 10.1080/15376490701672732

Taylor & Francis
Taylor & Francis Group

Analysis of Functionally Graded Plates by a Robust Meshless Method

A. J. M. Ferreira, C. M. C. Roque, and R. M. N. Jorge
Universidade do Porto, Portugal

G. E. Fasshauer
Illinois Institute of Technology, Chicago, IL, USA

R. C. Batra
Virginia Polytechnic Institute and State University, Blacksburg, VA, USA

The analysis of static deformations of functionally graded plates is performed by using the collocation method, the radial basis functions and a higher-order shear deformation theory. The collocation method is truly meshless, allowing a fast and simple domain and boundary discretization. We select the shape parameter in the radial basis functions by an optimization procedure based on the cross-validation technique, and use the Mori-Tanaka homogenization technique to deduce effective properties of functionally graded materials. Numerical tests show that the method is reliable, robust and produces accurate results.

Keywords meshfree method, radial basis functions, shape parameter optimization, third-order shear deformation theory

1. INTRODUCTION

In this paper, we use a meshless collocation method based on the radial basis functions (RBFs) for analysing static deformations of functionally graded (FG) plates with the shape parameter in the basis function optimized adaptively.

The RBFs were first used by Hardy [1,2] for the interpolation of geographical scattered data and later used by Kansa [3,4] for the solution of partial differential equations (PDEs). Many RBFs are reviewed in Liu [5], Fasshauer [6], Powell [7], and Wendland [8, 9], among others. The method has also been applied to the analysis of several engineering problems [10–12].

In functionally graded materials (FGMs), material properties vary continuously as opposed to those in laminated composites where such variation is discontinuous at layer interfaces. In an FGM the material properties are varied by changing the volume fractions of the constituents. An example of such materials is a FG coating deposited on top of a metallic substrate [13, 14]. FG plates have been studied by several authors [15–24] analytically [25] and by using either first-order or third-order shear deformation plate theories (FSDT or TSDT respectively) and finite element interpolation. Here we study FG plates by using a TSDT [15] and an interpolation scheme based on global multiquadrics [3, 4, 26–28]. The TSDT includes some of the assumptions of the classical plate theory by expanding the in-plane FSDT displacements (u, v) as a cubic function of the thickness coordinate.

The FG plate is assumed to be made of two interspaced isotropic constituents and the macroscopic response of the plate is assumed to be isotropic. Furthermore, the volume fractions of the two constituents are assumed to vary in the thickness direction only.

Meshless methods such as the element-free Galerkin [29,30], hp-clouds [31], the diffuse element [32], the partition of unity finite element [33], the natural element [34] and the meshless local Petrov-Galerkin [35, 36] have gained popularity for finding approximate solutions of boundary-value problems due to the ease of node placement and accuracy of computed results. The present global RBF method [3,4,28] neither requires a mesh nor evaluation of domain integrals, rather it interpolates by the collocation method the differential equations of the problem. The essential boundary conditions are easily satisfied by collocation at the boundary nodes. This approach has been successfully applied to the analysis of engineering problems [10, 11, 27]. Recently the RBF method was applied with excellent results to composite beams and plates [37, 38].

In previous research by the authors the shape parameter in the global RBFs was selected based on trial and error. Here we select this shape (or shift) parameter adaptively based on the cross-validation technique, suggested by Rippa [39].

The rest of the paper is organized as follows. Section 2 gives a formulation of the RBF method, and Section 3 a strategy to find the optimal value of the shape parameter in RBFs.

Received 28 March 2007; accepted 7 May 2007.
Address correspondence to A. J. M. Ferreira, Department of Mechanical and Industrial Engineering, University of Porta, Rua Dr. Roberto Frias, 4200-465 Porto, Portugal. E-mail: ferreira@fe.up.pt

Section 4 introduces the interpolation of governing equations and boundary conditions. Section 5 illustrates how to interpolate the boundary-value problem (BVP) with RBFs. Results of the analysis of static deformations of a simply-supported square FG plate are presented in Section 6 and compared with solutions obtained from other methods. Conclusions are summarized in Section 7.

2. THE RADIAL BASIS FUNCTION (RBF) METHOD

The RBF method relies on the Euclidean distance between two points and in some cases also on a user-defined shape parameter that is the object of various discussions. The value of this parameter not only defines the RBFs but also may make the resulting algebraic problem ill-conditioned giving poor quality solutions.

The numerical solution of partial differential equations (PDEs) is traditionally found by finite element methods, finite volume methods or finite difference methods. All of these methods are based on local interpolation strategies and depend on a mesh for local approximation. In these methods although the interpolation functions are continuous across inter-element boundaries, some of their partial derivatives are generally discontinuous [40–42].

An alternative approach for solving PDEs is based on generally discontinuous RBFs. An RBF depends only on the distance between two points and is of the form $g(\|\mathbf{x}_j - \mathbf{x}\|)$ where $\|\mathbf{x}_j - \mathbf{x}\|$ is the Euclidean norm. The RBF may also depend on a shape parameter c, in which case $g(\|\mathbf{x}_j - \mathbf{x}\|)$ is replaced by $g(\|\mathbf{x}_j - \mathbf{x}\|, c)$ [3,4,6,27,28,43].

Consider a set of nodes $x_1, x_2, \ldots, x_N \in \Omega \subset \mathbb{R}^n$. The radial basis functions centered at $\mathbf{x}_j$ are defined as

$$g_j(\mathbf{x}) \equiv g(\|\mathbf{x}_j - \mathbf{x}\|) \in \mathbb{R}^n, \quad j = 1, \ldots, N \tag{1}$$

Some of the most common RBFs are [3,4,6,27,28]:

$$\textbf{Multiquadrics}: g_j(\mathbf{x}) = (\|\mathbf{x}_j - \mathbf{x}\| + c^2)^{\frac{1}{2}} \tag{2}$$

$$\textbf{Inverse Multiquadrics}: g_j(\mathbf{x}) = (\|\mathbf{x}_j - \mathbf{x}\| + c^2)^{-\frac{1}{2}} \tag{3}$$

$$\textbf{Gaussians}: g_j(\mathbf{x}) = e^{-c^2\|\mathbf{x}_j - \mathbf{x}\|^2} \tag{4}$$

$$\textbf{Thin Plate Splines}: g_j(\mathbf{x}) = \|\mathbf{x}_j - \mathbf{x}\|^2 \log \|\mathbf{x}_j - \mathbf{x}\| \tag{5}$$

where c is a user-defined shape parameter. Here we use the multiquadric RBFs and select c adaptively.

The RBFs are insensitive to spatial dimensions, making the implementation of the method much easier than that of, e.g., finite elements [3,4]. An important feature of the RBF method is that it does not require a mesh. The only geometric properties needed in a RBF approximation are the distances between two points. Working with higher dimensional problems is not difficult as distances are easy to compute in any number of space dimensions.

Here we use Kansa's unsymmetric collocation method [3,4]. Consider a boundary-value problem defined on a domain $\Omega \subset \mathbb{R}^n$ and a linear elliptic PDE of the form

$$Lu(x) = \Lambda(x) \subset \mathbb{R}^n \tag{6}$$

$$Bu(x)_{|\partial\Omega} = \Xi(x) \in \mathbb{R}^n \tag{7}$$

where $\partial\Omega$ represents the boundary of the domain Ω. We use N_B points on the boundary ($\mathbf{x}_j$, $j = 1, \ldots, N_B$) and $(N - N_B)$ points in the interior ($\mathbf{x}_j$, $j = N_B + 1, \ldots, N$).

Let the RBF interpolant to the solution $u(\mathbf{x})$ be

$$s(\mathbf{x}, c) = \sum_{j=1}^{N} \alpha_j g(\|\mathbf{x}_j - \mathbf{x}\|, c) \tag{8}$$

Collocation of the boundary data at boundary points and of the PDE at interior points leads to the following equations:

$$s_B(\mathbf{x}_i, c) \equiv \sum_{j=1}^{N} \alpha_j B g(\|\mathbf{x}_j - \mathbf{x}_i\|, c) = \Lambda(\mathbf{x}_i), i = 1, \ldots, N_B \tag{9}$$

$$s_L(\mathbf{x}_i, c) \equiv \sum_{j=1}^{N} \alpha_j L g(\|\mathbf{x}_j - \mathbf{x}_i\|, c) = \Xi(\mathbf{x}_i), i = N_B + 1, \ldots, N \tag{10}$$

where $\Lambda(\mathbf{x}_i)$ and $\Xi(\mathbf{x}_i)$ are computed from the given functions $\Lambda(\mathbf{x})$ and $\Xi(\mathbf{x})$ respectively. Equations (9) and (10) can be written in the matrix form as

$$\begin{bmatrix} B\mathbf{g} \\ L\mathbf{g} \end{bmatrix} [\alpha] = \begin{bmatrix} \Lambda \\ \Xi \end{bmatrix} \tag{11}$$

or

$$\left[\mathcal{L}\right][\alpha] = \left[\lambda\right] \tag{12}$$

It has been shown that for inappropriate values of c, the unsymmetric coefficient matrix $\mathcal{L}$ can become ill-conditioned or even singular [44].

Here we compute an optimal value of the shape parameter c that does not solve the ill-conditioning issue, but avoids the trial and error technique.

3. COMPUTING AN OPTIMAL c

An optimal shape parameter c can be obtained for an interpolation problem $A\alpha = f$, $A = g(||\mathbf{x}_j - \mathbf{x}_i, c||)$, by the leave-one-out cross validation technique in regression analysis. The problem can be formulated as finding c in order to minimize a cost function given by the norm of an error vector $E(c)$ with

components

$$E_i(c) = f_i - \sum_{j=1, j\neq i}^{N} \alpha_j^{(i)} g(||\mathbf{x}_j - \mathbf{x}_i, c||) \tag{13}$$

Here $\sum_{j=1, j\neq i}^{N} \alpha_j^{(i)} g(||\mathbf{x}_j - \mathbf{x}_i, c||)$ is the function value predicted at the i-th data point using RBF interpolation based on a set of data that excludes the i-th point. From a computational point of view this cross-validation method appears to be very costly.

However, Rippa [39] has shown that this algorithm requires on the order of N^3 operations—the same order of operations required to solve the linear system for the interpolation problem.

According to Rippa the components of the error vector can be computed—for an interpolation problem—by the following more efficient formula:

$$E_i(c) = \frac{\alpha_i}{A_{i,i}^{-1}} \tag{14}$$

where α_i is the i-th coefficient for the full interpolation problem and $A_{i,i}^{-1}$ is the i-th diagonal element of the inverse of the corresponding interpolation matrix A. The same formula seems to have been found by Wang [45]. While Rippa tried different norms in his experiments and concluded that the ℓ_1-norm of the error vector leads to a better prediction of the optimal c-value, Wang used the ℓ_2-norm. Our numerical results below are based on the use of the ℓ_1-norm.

However, both methods mentioned above use an interpolation technique and rely on data given by a function f. In our boundary-value problem (BVP) we have a set of partial differential equations in the domain and a set of boundary conditions on the boundary nodes.

Since the only "data" we are given come from the right side λ in Eq. (12) we cannot base the error vector for the cross-validation algorithm on an actual error. Instead, we use the residual error, i.e.,

$$E_i(c) = \lambda_i - \sum_{j=1, j\neq i}^{N} \alpha_j^{(i)} \mathcal{L} g(||\mathbf{x}_j - \mathbf{x}_i, c||) \tag{15}$$

This idea is quite natural and its use has been justified before in the context of greedy adaptive algorithms for both RBF interpolation and collocation problems [46, 47] and as a guide for finding an optimal shape parameter for collocation problems [48].

Now the generalization of the Rippa cross-validation algorithm is straightforward. Our BVP is given by Eq. (12). We can use the following formula that is analogous to Eq. (14):

$$E_i(c) = \frac{\alpha_i}{\mathcal{L}_{i,i}^{-1}} \tag{16}$$

where α_i is the i-th coefficient for the full collocation problem (12) and $\mathcal{L}_{i,i}^{-1}$ is the i-th diagonal element of the inverse of the corresponding collocation matrix $\mathcal{L}$. Having the cost function, we use the MATLAB function fminbnd to find a local minimum.

The present approach provides excellent results for static deformations of FG plates, as can be seen from results presented in Section 6.

4. THIRD-ORDER SHEAR DEFORMATION PLATE THEORY (TSDT)

The TSDT [49] is based on the same assumptions as the classical plate theory and the FSDT, except that the assumption of straightness and normality of a transverse normal after deformation is relaxed by expanding the in-plane displacements (u, v) as cubic functions of the thickness coordinate. That is, the displacement field is written as

$$u(x, y, z) = u_o(x, y) + z\theta_x(x, y) - \frac{4}{3h^2} z^3 \left(\theta_x(x, y) + \frac{\partial w_o(x, y)}{\partial x} \right) \tag{17}$$

$$v(x, y, z) = v_o(x, y) + z\theta_y(x, y) - \frac{4}{3h^2} z^3 \left(\theta_y(x, y) + \frac{\partial w_o(x, y)}{\partial y} \right) \tag{18}$$

$$w(x, y, z) = w_o(x, y) \tag{19}$$

For infinitesimal deformations, the strain-displacement relations are:

$$\epsilon_{xx} = \frac{\partial u}{\partial x},\ \epsilon_{yy} = \frac{\partial v}{\partial y},\ \gamma_{xy} = \frac{\partial u}{\partial y} + \frac{\partial v}{\partial x},$$
$$\gamma_{xz} = \frac{\partial u}{\partial z} + \frac{\partial w}{\partial x},\ \gamma_{yz} = \frac{\partial v}{\partial z} + \frac{\partial w}{\partial y} \tag{20}$$

Thus strains can be expressed as

$$\begin{Bmatrix} \epsilon_{xx} \\ \epsilon_{yy} \\ \gamma_{xy} \end{Bmatrix} = \begin{Bmatrix} \epsilon_{xx}^{(0)} \\ \epsilon_{yy}^{(0)} \\ \gamma_{xy}^{(0)} \end{Bmatrix} + z \begin{Bmatrix} \epsilon_{xx}^{(1)} \\ \epsilon_{yy}^{(1)} \\ \gamma_{xy}^{(1)} \end{Bmatrix} + z^3 \begin{Bmatrix} \epsilon_{xx}^{(3)} \\ \epsilon_{yy}^{(3)} \\ \gamma_{xy}^{(3)} \end{Bmatrix} \tag{21}$$

$$\begin{Bmatrix} \gamma_{xz} \\ \gamma_{yz} \end{Bmatrix} = \begin{Bmatrix} \gamma_{xz}^{(0)} \\ \gamma_{yz}^{(0)} \end{Bmatrix} + z^2 \begin{Bmatrix} \gamma_{xz}^{(2)} \\ \gamma_{yz}^{(2)} \end{Bmatrix} \tag{22}$$

where

$$\begin{Bmatrix} \epsilon_{xx}^{(0)} \\ \epsilon_{yy}^{(0)} \\ \gamma_{xy}^{(0)} \end{Bmatrix} = \begin{Bmatrix} \dfrac{\partial u_o}{\partial x} \\ \dfrac{\partial v_o}{\partial y} \\ \dfrac{\partial u_o}{\partial y} + \dfrac{\partial v_o}{\partial x} \end{Bmatrix} \tag{23}$$

$$\begin{Bmatrix} \epsilon_{xx}^{(1)} \\ \epsilon_{yy}^{(1)} \\ \gamma_{xy}^{(1)} \end{Bmatrix} = \begin{Bmatrix} \dfrac{\partial \theta_x}{\partial x} \\ \dfrac{\partial \theta_y}{\partial y} \\ \dfrac{\partial \theta_x}{\partial y} + \dfrac{\partial \theta_y}{\partial x} \end{Bmatrix} \tag{24}$$

$$\begin{Bmatrix} \epsilon_{xx}^{(3)} \\ \epsilon_{yy}^{(3)} \\ \gamma_{xy}^{(3)} \end{Bmatrix} = -c_1 \begin{Bmatrix} \dfrac{\partial \theta_x}{\partial x} + \dfrac{\partial^2 w_o}{\partial x^2} \\ \dfrac{\partial \theta_y}{\partial y} + \dfrac{\partial^2 w_o}{\partial y^2} \\ \dfrac{\partial \theta_x}{\partial y} + \dfrac{\partial \theta_y}{\partial x} + 2\dfrac{\partial^2 w_o}{\partial x \partial y} \end{Bmatrix} \tag{25}$$

$$\begin{Bmatrix} \gamma_{xz}^{(0)} \\ \gamma_{yz}^{(0)} \end{Bmatrix} = \begin{Bmatrix} \dfrac{\partial w_o}{\partial x} + \theta_x \\ \dfrac{\partial w_o}{\partial y} + \theta_y \end{Bmatrix} \tag{26}$$

$$\begin{Bmatrix} \gamma_{xz}^{(2)} \\ \gamma_{yz}^{(2)} \end{Bmatrix} = -c_2 \begin{Bmatrix} \dfrac{\partial w_o}{\partial x} + \theta_x \\ \dfrac{\partial w_o}{\partial y} + \theta_y \end{Bmatrix} \tag{27}$$

and $c_1 = \frac{4}{3h^2}$, $c_2 = 3c_1$.

The equilibrium equations of the TSDT are derived from the principle of virtual displacements. The virtual strain energy δU, and the virtual work done by applied forces δV are given by

$$\begin{aligned} \delta U = & \int_{\Omega_0} \left\{ \int_{-h/2}^{h/2} \Big[\sigma_{xx} \left(\delta\epsilon_{xx}^{(0)} + z\delta\epsilon_{xx}^{(1)} - c_1 z^3 \delta\epsilon_{xx}^{(3)} \right) \right. \\ & + \sigma_{yy} \left(\delta\epsilon_{yy}^{(0)} + z\delta\epsilon_{yy}^{(1)} - c_1 z^3 \delta\epsilon_{yy}^{(3)} \right) \\ & + \tau_{xy} \left(\delta\gamma_{xy}^{(0)} + z\delta\gamma_{xy}^{(1)} - c_1 z^3 \delta\gamma_{xy}^{(3)} \right) + \tau_{xz} \\ & \left. \times (\delta\gamma_{xz}^{(0)} + z^2 \delta\gamma_{xz}^{(2)}) + \tau_{yz} \left(\delta\gamma_{yz}^{(0)} + z^2 \delta\gamma_{yz}^{(2)} \right) \Big] dz \right\} dx\, dy \\ = & \int_{\Omega_0} \Big(N_{xx} \delta\epsilon_{xx}^{(0)} + M_{xx} \delta\epsilon_{xx}^{(1)} - c_1 P_{xx} \delta\epsilon_{xx}^{(3)} + N_{yy} \delta\epsilon_{yy}^{(0)} \\ & + M_{yy} \delta\epsilon_{yy}^{(1)} - c_1 P_{yy} \delta\epsilon_{yy}^{(3)} + N_{xy} \delta\gamma_{xy}^{(0)} \\ & + M_{xy} \delta\gamma_{xy}^{(1)} - c_1 P_{xy} \delta\gamma_{xy}^{(3)} + Q_x \delta\gamma_{xz}^{(0)} + R_x \delta\gamma_{xz}^{(2)} \\ & + Q_y \delta\gamma_{yz}^{(0)} + R_y \delta\gamma_{yz}^{(2)} \Big) dx\, dy \end{aligned} \tag{28}$$

and

$$\delta V = -\int_{\Omega_0} q \delta w_o \, dx dy \tag{29}$$

where Ω_0 denotes the midplane of the laminate, q is the resultant of the external distributed load applied on the top and the bottom surfaces of the plate, and

$$\begin{Bmatrix} N_{\alpha\beta} \\ M_{\alpha\beta} \\ P_{\alpha\beta} \end{Bmatrix} = \int_{-h/2}^{h/2} \sigma_{\alpha\beta} \begin{Bmatrix} 1 \\ z \\ z^3 \end{Bmatrix} dz \tag{30}$$

$$\begin{Bmatrix} Q_\alpha \\ R_\alpha \end{Bmatrix} = \int_{-h/2}^{h/2} \sigma_{\alpha z} \begin{Bmatrix} 1 \\ z^2 \end{Bmatrix} dz \tag{31}$$

where α, β take the symbols x, y.

Substituting for δU and δV into the virtual work statement $\delta U - \delta V = 0$, noting that the virtual strains can be expressed in terms of the generalized displacements, integrating by parts to transfer derivatives from the generalized virtual displacements to the corresponding kinetic variables, and using the fundamental lemma of the calculus of variations, we obtain the following Euler-Lagrange equations [50]:

$$\begin{aligned} \frac{\partial N_{xx}}{\partial x} + \frac{\partial N_{xy}}{\partial y} &= 0 \\ \frac{\partial N_{xy}}{\partial x} + \frac{\partial N_{yy}}{\partial y} &= 0 \\ \frac{\partial \overline{Q}_x}{\partial x} + \frac{\partial \bar{Q}_y}{\partial y} + q &= 0 \\ \frac{\partial \bar{M}_{xx}}{\partial x} + \frac{\partial \bar{M}_{xy}}{\partial y} - \bar{Q}_x &= 0 \\ \frac{\partial \bar{M}_{xy}}{\partial x} + \frac{\partial \bar{M}_{yy}}{\partial y} - \bar{Q}_y &= 0 \end{aligned} \tag{32}$$

with

$$\bar{M}_{\alpha\beta} = M_{\alpha\beta} - \frac{4}{3h^2} P_{\alpha\beta} \tag{33}$$

$$\bar{Q}_\alpha = Q_\alpha - \frac{4}{h^2} R_\alpha \tag{34}$$

The stress-strain relations for a linear elastic isotropic plate with $\sigma_{zz} = 0$ are

$$\begin{Bmatrix} \sigma_x \\ \sigma_y \\ \tau_{yx} \\ \tau_{yz} \\ \tau_{xz} \end{Bmatrix} = \begin{bmatrix} Q_{11} & Q_{12} & 0 & 0 & 0 \\ Q_{12} & Q_{11} & 0 & 0 & 0 \\ 0 & 0 & Q_{33} & 0 & 0 \\ 0 & 0 & 0 & Q_{44} & 0 \\ 0 & 0 & 0 & 0 & Q_{55} \end{bmatrix} \begin{Bmatrix} \varepsilon_x \\ \varepsilon_y \\ \gamma_{yx} \\ \gamma_{yz} \\ \gamma_{xz} \end{Bmatrix} \tag{35}$$

where the elastic constants Q_{ij} are given by

$$\begin{aligned} Q_{11} = \frac{E}{1-\nu^2}; \quad Q_{12} = \frac{\nu E}{1-\nu^2}; \\ Q_{33} = Q_{44} = Q_{55} = \frac{E}{2(1+\nu)} \end{aligned} \tag{36}$$

E is Young's modulus and ν Poisson's ratio.

The material properties E and ν at a point are determined by the Mori-Tanaka homogenization technique. For a random distribution of isotropic particles in an isotropic matrix, the bulk modulus K, and the shear modulus G are given by

$$\frac{K-K_1}{K_2-K_1}=\frac{V_2}{1+(1-V_2)\frac{K_2-K_1}{K_1+\frac{4}{3}G_1}} \tag{37}$$

$$\frac{G-G_1}{G_2-G_1}=\frac{V_2}{1+(1-V_2)\frac{G_2-G_1}{G_1+f_1}} \tag{38}$$

where $f_1=\frac{G_1(9K_1+8G_1)}{6(K_1+2G_1)}$ and subscripts 1 and 2 represent the ceramic and the metal phases respectively. Young's modulus and Poisson's ratio are related to the bulk and the shear moduli by

$$K=\frac{E}{3(1-2\nu)} \tag{39}$$

$$G=\frac{E}{2(1+\nu)} \tag{40}$$

It is assumed that the volume fraction of the ceramic phase varies only in the thickness direction according to the relation $V_1=(\frac{1}{2}+\frac{z}{h})^p$, where p is an exponent factor, h the plate thickness, and $-h/2\le z\le h/2$.

The Euler-Lagrange equations (32) written in terms of displacements by substituting for strains from Eqs. (21)–(27), stress resultants from Eqs. (30), (31), (33) and (34), and stresses from Eq. (35) are

$$\begin{aligned}
&A_{11}\frac{\partial^2 u_o}{\partial x^2}+A_{12}\frac{\partial^2 v_o}{\partial y\partial x}+B_{11}\frac{\partial^2\theta_x}{\partial x^2}+B_{12}\frac{\partial^2\theta_y}{\partial y\partial x}\\
&-\frac{4}{3h^2}E_{11}\left(\frac{\partial^2\theta_x}{\partial x^2}+\frac{\partial^3 w_o}{\partial x^3}\right)-\frac{4}{3h^2}E_{12}\left(\frac{\partial^2\theta_y}{\partial y\partial x}+\frac{\partial^3 w_o}{\partial y^2\partial x}\right)\\
&+A_{33}\left(\frac{\partial^2 u_o}{\partial y^2}+\frac{\partial^2 v_o}{\partial y\partial x}\right)+B_{33}\left(\frac{\partial^2\theta_x}{\partial y^2}+\frac{\partial^2\theta_y}{\partial y\partial x}\right)\\
&-\frac{4}{3h^2}E_{33}\left(\frac{\partial^2\theta_x}{\partial y^2}+\frac{\partial^2\theta_y}{\partial y\partial x}+2\frac{\partial^3 w_o}{\partial y^2\partial x}\right)=0
\end{aligned} \tag{41}$$

$$\begin{aligned}
&A_{33}\left(\frac{\partial^2 u_o}{\partial y\partial x}+\frac{\partial^2 v_o}{\partial x^2}\right)+B_{33}\left(\frac{\partial^2\theta_x}{\partial y\partial x}+\frac{\partial^2\theta_y}{\partial x^2}\right)\\
&-\frac{4}{3h^2}E_{33}\left(\frac{\partial^2\theta_x}{\partial y\partial x}+\frac{\partial^2\theta_y}{\partial x^2}+2\frac{\partial^3 w_o}{\partial y\partial x^2}\right)+A_{12}\frac{\partial^2 u_o}{\partial y\partial x}\\
&+A_{22}\frac{\partial^2 v_o}{\partial y^2}+B_{12}\frac{\partial^2\theta_x}{\partial y\partial x}+B_{22}\frac{\partial^2\theta_y}{\partial y^2}\\
&-\frac{4}{3h^2}E_{12}\left(\frac{\partial^2\theta_x}{\partial y\partial x}+\frac{\partial^3 w_o}{\partial y\partial x^2}\right)\\
&-\frac{4}{3h^2}E_{22}\left(\frac{\partial^2\theta_y}{\partial y^2}+\frac{\partial^3 w_o}{\partial y^3}\right)=0
\end{aligned} \tag{42}$$

$$\begin{aligned}
&A_{55}\left(\frac{\partial\theta_x}{\partial x}+\frac{\partial^2 w_o}{\partial x^2}\right)-\frac{8}{h^2}D_{55}\left(\frac{\partial\theta_x}{\partial x}+\frac{\partial^2 w_o}{\partial x^2}\right)\\
&+\frac{16}{h^4}F_{55}\left(\frac{\partial\theta_x}{\partial x}+\frac{\partial^2 w_o}{\partial x^2}\right)+A_{44}\left(\frac{\partial\theta_y}{\partial y}+\frac{\partial^2 w_o}{\partial y^2}\right)\\
&-\frac{8}{h^2}D_{44}\left(\frac{\partial\theta_y}{\partial y}+\frac{\partial^2 w_o}{\partial y^2}\right)+\frac{16}{h^4}F_{44}\left(\frac{\partial\theta_y}{\partial y}+\frac{\partial^2 w_o}{\partial y^2}\right)\\
&+\frac{4}{3}\Bigg[E_{11}\frac{\partial^3 u_o}{\partial x^3}+E_{12}\frac{\partial^3 v_o}{\partial y\partial x^2}+F_{11}\frac{\partial^3\theta_x}{\partial x^3}+F_{12}\frac{\partial^3\theta_y}{\partial y\partial x^2}\\
&-\frac{4}{3h^2}H_{11}\left(\frac{\partial^3\theta_x}{\partial x^3}+\frac{\partial^4 w_o}{\partial x^4}\right)-\frac{4}{3h^2}H_{12}\left(\frac{\partial^3\theta_y}{\partial y\partial x^2}+\frac{\partial^4 w_o}{\partial y^2\partial x^2}\right)\\
&+2E_{33}\left(\frac{\partial^3 u_o}{\partial y^2\partial x}+\frac{\partial^3 v_o}{\partial y\partial x^2}\right)+2F_{33}\left(\frac{\partial^3\theta_x}{\partial y^2\partial x}+\frac{\partial^3\theta_y}{\partial y\partial x^2}\right)\\
&-\frac{8}{3h^2}H_{33}\left(\frac{\partial^3\theta_x}{\partial y^2\partial x}+\frac{\partial^3\theta_y}{\partial y\partial x^2}+2\frac{\partial^4 w_o}{\partial y^2\partial x^2}\right)+E_{12}\frac{\partial^3 u_o}{\partial y^2\partial x}\\
&+E_{22}\frac{\partial^3 v_o}{\partial y^3}+F_{12}\frac{\partial^3\theta_x}{\partial y^2\partial x}+F_{22}\frac{\partial^3\theta_y}{\partial y^3}-\frac{4}{3h^2}H_{12}\Bigg(\frac{\partial^3\theta_x}{\partial y^2\partial x}\\
&+\frac{\partial^4 w_o}{\partial y^2\partial x^2}\Bigg)-\frac{4}{3h^2}H_{22}\left(\frac{\partial^3\theta_y}{\partial y^3}+\frac{\partial^4 w_o}{\partial y^4}\right)\Bigg]\frac{1}{h^2}=-q
\end{aligned} \tag{43}$$

$$\begin{aligned}
&-A_{55}\left(\theta_x+\frac{\partial w_o}{\partial x}\right)+\frac{8}{h^2}D_{55}\left(\theta_x+\frac{\partial w_o}{\partial x}\right)\\
&-\frac{16}{h^4}F_{55}\left(\theta_x+\frac{\partial w_o}{\partial x}\right)+B_{11}\frac{\partial^2 u_o}{\partial x^2}+B_{12}\frac{\partial^2 v_o}{\partial y\partial x}+D_{11}\frac{\partial^2\theta_x}{\partial x^2}\\
&+D_{12}\frac{\partial^2\theta_y}{\partial y\partial x}\frac{4}{3h^2}F_{11}\left(\frac{\partial^2\theta_x}{\partial x^2}+\frac{\partial^3 w_o}{\partial x^3}\right)\\
&-\frac{4}{3h^2}F_{12}\left(\frac{\partial^2\theta_y}{\partial y\partial x}+\frac{\partial^3 w_o}{\partial y^2\partial x}\right)-\frac{4}{3}\Bigg[E_{11}\frac{\partial^2 u_o}{\partial x^2}+E_{12}\frac{\partial^2 v_o}{\partial y\partial x}\\
&+F_{11}\frac{\partial^2\theta_x}{\partial x^2}+F_{12}\frac{\partial^2\theta_y}{\partial y\partial x}-\frac{4}{3h^2}H_{11}\left(\frac{\partial^2\theta_x}{\partial x^2}+\frac{\partial^3 w_o}{\partial x^3}\right)\\
&-\frac{4}{3h^2}H_{12}\left(\frac{\partial^2\theta_y}{\partial y\partial x}+\frac{\partial^3 w_o}{\partial y^2\partial x}\right)\Bigg]\frac{1}{h^2}+B_{33}\left(\frac{\partial^2 u_o}{\partial y^2}+\frac{\partial^2 v_o}{\partial y\partial x}\right)\\
&+D_{33}\left(\frac{\partial^2\theta_x}{\partial y^2}+\frac{\partial^2\theta_y}{\partial y\partial x}\right)\\
&-\frac{4}{3h^2}F_{33}\left(\frac{\partial^2\theta_x}{\partial y^2}+\frac{\partial^2\theta_y}{\partial y\partial x}+2\frac{\partial^3 w_o}{\partial y^2\partial x}\right)\\
&-\frac{4}{3}\Bigg[B_{33}\left(\frac{\partial^2 u_o}{\partial y^2}+\frac{\partial v_o}{\partial y\partial x}\right)+F_{33}\left(\frac{\partial^2\theta_x}{\partial y^2}+\frac{\partial^2\theta_y}{\partial y\partial x}\right)\\
&-\frac{4}{3h^2}H_{33}\left(\frac{\partial^2\theta_x}{\partial y^2}+\frac{\partial^2\theta_y}{\partial y\partial x}+2\frac{\partial^3 w_o}{\partial y^2\partial x}\right)\Bigg]\frac{1}{h^2}=0
\end{aligned} \tag{44}$$

$$\begin{aligned}
&-A_{44}\left(\theta_y+\frac{\partial w_o}{\partial y}\right)+\frac{8}{h^2}D_{44}\left(\theta_y+\frac{\partial w_o}{\partial y}\right)\\
&-\frac{16}{h^4}F_{44}\left(\theta_y+\frac{\partial w_o}{\partial y}\right)+B_{12}\frac{\partial^2 u_o}{\partial y\partial x}+B_{22}\frac{\partial^2 v_o}{\partial y^2}\\
&+D_{12}\frac{\partial^2\theta_x}{\partial y\partial x}+D_{22}\frac{\partial^2\theta_y}{\partial y^2}-\frac{4}{3h^2}F_{12}\left(\frac{\partial^2\theta_x}{\partial y\partial x}+\frac{\partial^3 w_o}{\partial y\partial x^2}\right)
\end{aligned}$$

$$
\begin{aligned}
&- \frac{4}{3h^2}F_{22}\left(\frac{\partial^2\theta_y}{\partial y^2}+\frac{\partial^3 w_o}{\partial y^3}\right)\frac{4}{3}\Bigg[E_{12}\frac{\partial^2 u_o}{\partial y\partial x}+E_{22}\frac{\partial^2 v_o}{\partial y^2}\\
&+F_{12}\frac{\partial^2\theta_x}{\partial y\partial x}+F_{22}\frac{\partial^2\theta_y}{\partial y^2}-\frac{4}{3h^2}H_{12}\left(\frac{\partial^2\theta_x}{\partial y\partial x}+\frac{\partial^3 w_o}{\partial y\partial x^2}\right)\\
&-\frac{4}{3h^2}H_{22}\left(\frac{\partial^2\theta_y}{\partial y^2}+\frac{\partial^3 w_o}{\partial y^3}\right)\Bigg]\frac{1}{h^2}+B_{33}\left(\frac{\partial^2 u_o}{\partial y\partial x}+\frac{\partial^2 v_o}{\partial x^2}\right)\\
&+D_{33}\left(\frac{\partial^2\theta_x}{\partial y\partial x}+\frac{\partial^2\theta_y}{\partial x^2}\right)\\
&-\frac{4}{3h^2}F_{33}\left(\frac{\partial^2\theta_x}{\partial y\partial x}+\frac{\partial^2\theta_y}{\partial x^2}+2\frac{\partial^3 w_o}{\partial y\partial x^2}\right)\\
&-\frac{4}{3}\Bigg[E_{33}\left(\frac{\partial^2 u_o}{\partial y\partial x}+\frac{\partial^2 v_o}{\partial x^2}\right)+F_{33}\left(\frac{\partial^2\theta_x}{\partial y\partial x}+\frac{\partial^2\theta_y}{\partial x^2}\right)\\
&-\frac{4}{3h^2}H_{33}\left(\frac{\partial^2\theta_x}{\partial y\partial x}+\frac{\partial^2\theta_y}{\partial x^2}+2\frac{\partial^3 w_o}{\partial y\partial x^2}\right)\Bigg]\frac{1}{h^2}=0 \qquad (45)
\end{aligned}
$$

where

$$
(A_{ij}, B_{ij}, D_{ij}, E_{ij}, F_{ij}, H_{ij}) = \int_{-\frac{h}{2}}^{\frac{h}{2}} Q_{ij}(1, z, z^2, z^3, z^4, z^6)dz \qquad (46)
$$

5. INTERPOLATION WITH RADIAL BASIS FUNCTIONS

Using the RBFs, the governing differential Eqs. (41)–(45) are interpolated, at each node i, as

$$
\begin{aligned}
&\sum_{j=1}^{N}\alpha_j^{u_o}\left[A_{11}\frac{\partial^2 g_j}{\partial x^2}+A_{33}\frac{\partial^2 g_j}{\partial y^2}\right]+\sum_{j=1}^{N}\alpha_j^{v_o}\left[(A_{12}+A_{33})\frac{\partial^2 g_j}{\partial y\partial x}\right]\\
&\quad+\sum_{j=1}^{N}\alpha_j^{w_o}\left[\left(-\frac{8}{3h^2}E_{33}-\frac{4}{3h^2}E_{12}\right)\frac{\partial^3 g_j}{\partial y^2\partial x}-\frac{4}{3h^2}E_{11}\frac{\partial^3 g_j}{\partial x^3}\right]\\
&\quad+\sum_{j=1}^{N}\alpha_j^{\theta_x}\left[\left(B_{11}-\frac{4}{3h^2}E_{11}\right)\frac{\partial^2 g_j}{\partial x^2}+\left(B_{33}-\frac{4}{3h^2}E_{33}\right)\frac{\partial^2 g_j}{\partial y^2}\right]\\
&\quad+\sum_{j=1}^{N}\alpha_j^{\theta_y}\left[\left(B_{12}-\frac{4}{3h^2}E_{12}+B_{33}-\frac{4}{3h^2}E_{33}\right)\frac{\partial^2 g_j}{\partial y\partial x}\right]=0 \qquad (47)\\
&\sum_{j=1}^{N}\alpha_j^{u_o}\left[(A_{33}+A_{12})\frac{\partial^2 g_j}{\partial y\partial x}\right]+\sum_{j=1}^{N}\alpha_j^{v_o}\left[A_{33}\frac{\partial^2 g_j}{\partial x^2}+A_{22}\frac{\partial^2 g_j}{\partial y^2}\right]\\
&\quad+\sum_{j=1}^{N}\alpha_j^{w_o}\left[\left(-\frac{8}{3h^2}E_{33}-\frac{4}{3h^2}E_{12}\right)\frac{\partial^3 g_j}{\partial y\partial x^2}-\frac{4}{3h^2}E_{22}\frac{\partial^3 g_j}{\partial y^3}\right]\\
&\quad+\sum_{j=1}^{N}\alpha_j^{\theta_x}\left[\left(B_{33}-\frac{4}{3h^2}E_{33}+B_{12}-\frac{4}{3h^2}E_{12}\right)\frac{\partial^2 g_j}{\partial y\partial x}\right]\\
&\quad+\sum_{j=1}^{N}\alpha_j^{\theta_y}\left[\left(B_{33}-\frac{4}{3h^2}E_{33}\right)\frac{\partial^2 g_j}{\partial x^2}\right.\\
&\quad\left.+\left(B_{22}-\frac{4}{3h^2}E_{22}\right)\frac{\partial^2 g_j}{\partial y^2}\right]=0 \qquad (48)
\end{aligned}
$$

$$
\begin{aligned}
&\sum_{j=1}^{N}\alpha_j^{u_o}\left[\frac{4}{3h^2}E_{11}\frac{\partial^3 g_j}{\partial x^3}+\left(\frac{8}{3h^2}E_{33}+\frac{4}{3h^2}E_{12}\right)\frac{\partial^3 g_j}{\partial y^2\partial x}\right]\\
&\quad+\sum_{j=1}^{N}\alpha_j^{v_o}\left[\frac{4}{3h^2}E_{22}\frac{\partial^3 g_j}{\partial y^3}+\left(\frac{8}{3h^2}E_{33}+\frac{4}{3h^2}E_{12}\right)\frac{\partial^3 g_j}{\partial y\partial x^2}\right]\\
&\quad+\sum_{j=1}^{N}\alpha_j^{w_o}\left[-\frac{16}{9h^4}H_{11}\frac{\partial^4 g_j}{\partial x^4}-\frac{16}{9h^4}H_{22}\frac{\partial^4 g_j}{\partial y^4}\right.\\
&\quad+\left(-\frac{8}{h^2}D_{55}+\frac{16}{h^4}F_{55}+A_{55}\right)\frac{\partial^2 g_j}{\partial x^2}\\
&\quad+\left(-\frac{8}{h^2}D_{44}+\frac{16}{h^4}F_{44}+A_{44}\right)\frac{\partial^2 g_j}{\partial y^2}\\
&\quad\left.+\left(-\frac{32}{9h^4}H_{12}-\frac{64}{9h^4}H_{33}\right)\frac{\partial^4 g_j}{\partial x^2\partial y^2}\right]\\
&\quad+\sum_{j=1}^{N}\alpha_j^{\theta_x}\left[\left(A_{55}-\frac{8}{h^2}D_{55}+\frac{16}{h^4}F_{55}\right)\frac{\partial g_j}{\partial x}\right.\\
&\quad+\left(\frac{4}{3h^2}F_{11}-\frac{16}{9h^4}H_{11}\right)\frac{\partial^3 g_j}{\partial x^3}\\
&\quad\left.+\left(\frac{8}{3h^2}F_{33}+\frac{4}{3h^2}F_{12}-\frac{32}{9h^4}H_{33}-\frac{16}{9h^4}H_{12}\right)\frac{\partial^3 g_j}{\partial y^2\partial x}\right]\\
&\quad+\sum_{j=1}^{N}\alpha_j^{\theta_y}\left[\left(\frac{16}{h^4}F_{44}+A_{44}-\frac{8}{h^2}D_{44}\right)\frac{\partial g_j}{\partial y}\right.\\
&\quad+\left(\frac{4}{3h^2}F_{12}-\frac{16}{9h^4}H_{12}+\frac{8}{3h^2}F_{33}-\frac{32}{9h^4}H_{33}\right)\frac{\partial^3 g_j}{\partial x^2\partial y}\\
&\quad\left.+\left(\frac{4}{3h^2}F_{22}-\frac{16}{9h^4}H_{22}\right)\frac{\partial g_j}{\partial y^3}\right]=-q \qquad (49)\\
&\sum_{j=1}^{N}\alpha_j^{u_o}\left[\left(-\frac{4}{3h^2}E_{33}+E_{33}\right)\frac{\partial^2 g_j}{\partial y^2}\right.\\
&\quad\left.+\left(-\frac{4}{3h^2}E_{11}+B_{11}\right)\frac{\partial^2 g_j}{\partial x^2}\right]\\
&\quad+\sum_{j=1}^{N}\alpha_j^{v_o}\left[\left(-\frac{4}{3h^2}E_{33}-\frac{4}{3h^2}E_{12}+E_{33}+B_{12}\right)\frac{\partial^2 g_j}{\partial y\partial x}\right]\\
&\quad+\sum_{j=1}^{N}\alpha_j^{w_o}\left[\left(-\frac{4}{3h^2}F_{11}+\frac{16}{9h^4}H_{11}\right)\frac{\partial^3 g_j}{\partial x^3}\right.\\
&\quad+\left(-\frac{8}{3h^2}F_{33}+\frac{32}{9h^4}H_{33}+\frac{16}{9h^4}H_{12}-\frac{4}{3h^2}F_{12}\right)\frac{\partial^3 g_j}{\partial x\partial y^2}\\
&\quad\left.+\left(-\frac{16}{h^4}F_{55}+\frac{8}{h^2}D_{55}-A_{55}\right)\frac{\partial g_j}{\partial x}\right]\\
&\quad+\sum_{j=1}^{N}\alpha_j^{\theta_x}\left[\left(-\frac{8}{3h^2}F_{11}+\frac{16}{9h^4}H_{11}+D_{11}\right)\frac{\partial^2 g_j}{\partial x^2}\right.\\
&\quad\left.+\left(\frac{16}{9h^4}H_{33}-\frac{8}{3h^2}F_{33}+D_{33}\right)\frac{\partial^2 g_j}{\partial y^2}\right.
\end{aligned}
$$

$$+\left(-A_{55}-\frac{16}{h^4}F_{55}+\frac{8}{h^2}D_{55}\right)g_j\Bigg]$$
$$+\sum_{j=1}^{N}\alpha_j^{\theta_y}\Bigg[\left(\frac{16}{9h^4}H_{33}-\frac{8}{3h^2}F_{12}-\frac{8}{3h^2}F_{33}\right.$$
$$\left.+\frac{16}{9h^4}H_{12}+D_{33}+D_{12}\right)\frac{\partial^2 g_j}{\partial y\partial x}\Bigg]=0 \tag{50}$$
$$\sum_{j=1}^{N}\alpha_j^{u_o}\Bigg[\left(-\frac{4}{3h^2}E_{33}+E_{33}-\frac{4}{3h^2}E_{12}+B_{12}\right)\frac{\partial^2 g_j}{\partial x\partial y}\Bigg]$$
$$+\sum_{j=1}^{N}\alpha_j^{v_o}\Bigg[\left(-\frac{4}{3h^2}E_{22}+B_{22}\right)\frac{\partial^2 g_j}{\partial y^2}$$
$$+\left(-\frac{4}{3h^2}E_{33}+E_{33}\right)\frac{\partial^2 g_j}{\partial x^2}\Bigg]$$
$$+\sum_{j=1}^{N}\alpha_j^{w_o}\Bigg[\left(-\frac{4}{3h^2}F_{22}+\frac{16}{9h^4}H_{22}\right)\frac{\partial^3 g_j}{\partial y^3}$$
$$+\left(-\frac{4}{3h^2}F_{12}+\frac{16}{9h^4}H_{12}-\frac{8}{3h^2}F_{33}+\frac{32}{9h^4}H_{33}\right)\frac{\partial^3 g_j}{\partial y\partial x^2}$$
$$+\left(\frac{8}{h^2}D_{44}-\frac{16}{h^4}F_{44}-A_{44}\right)\frac{\partial g_j}{\partial y}\Bigg]$$
$$+\sum_{j=1}^{N}\alpha_j^{\theta_x}\Bigg[\left(\frac{16}{9h^4}H_{33}+D_{33}-\frac{8}{3h^2}F_{12}+\frac{16}{9h^4}H_{12}\right.$$
$$\left.-\frac{8}{3h^2}F_{33}+D_{12}\right)\frac{\partial^2 g_j}{\partial x\partial y}\Bigg]$$
$$+\sum_{j=1}^{N}\alpha_j^{\theta_y}\Bigg[\left(\frac{16}{9h^4}H_{22}-\frac{8}{3h^2}F_{22}+D_{22}\right)\frac{\partial^2 g_j}{\partial y^2}$$
$$+\left(D_{33}+\frac{16}{9h^4}H_{33}-\frac{8}{3h^2}F_{33}\right)\frac{\partial^2 g_j}{\partial x^2}$$
$$+\left(-A_{44}-\frac{16}{h^4}F_{44}+\frac{8}{h^2}D_{44}\right)g_j\Bigg]=0 \tag{51}$$

For each boundary node, we use the RBFs to interpolate the corresponding boundary condition. For example at a simply supported edge $x=a$ the five boundary conditions (note that in the following equations, g_j stands for $g_j\equiv g_j(x=a)$, for simplicity of notation)

$$w(x=a)=0 \tag{52}$$
$$v(x=a)=0 \tag{53}$$
$$\theta_y(x=a)=0 \tag{54}$$

$$N_{x\,(\mathrm{x=a})}=A_{11}\frac{\partial u_o}{\partial x}+A_{12}\frac{\partial v_o}{\partial y}+B_{11}\frac{\partial\theta_x}{\partial x}+B_{12}\frac{\partial\theta_y}{\partial y}$$
$$-\frac{4}{3h^2}E_{11}\left(\frac{\partial\theta_x}{\partial x}+\frac{\partial^2 w_o}{\partial x^2}\right)-\frac{4}{3h^2}E_{12}\left(\frac{\partial\theta_y}{\partial y}+\frac{\partial^2 w_o}{\partial y^2}\right)=0 \tag{55}$$

$$\bar{M}_{x\,(\mathrm{x=a})}=B_{11}\frac{\partial u_o}{\partial x}+B_{12}\frac{\partial v_o}{\partial y}+D_{11}\frac{\partial\theta_x}{\partial x}+D_{12}\frac{\partial\theta_y}{\partial y}$$
$$-\frac{4}{3h^2}F_{11}\left(\frac{\partial\theta_x}{\partial x}+\frac{\partial^2 w_o}{\partial x^2}\right)-\frac{4}{3h^2}F_{12}\left(\frac{\partial\theta_y}{\partial y}+\frac{\partial^2 w_o}{\partial y^2}\right)$$
$$-\frac{4}{3}\Bigg[E_{11}\frac{\partial u_o}{\partial x}+E_{12}\frac{\partial v_o}{\partial y}+F_{11}\frac{\partial\theta_x}{\partial x}+F_{12}\frac{\partial\theta_y}{\partial y}$$
$$-\frac{4}{3h^2}H_{11}\left(\frac{\partial\theta_x}{\partial x}+\frac{\partial^2 w_o}{\partial x^2}\right)$$
$$-\frac{4}{3h^2}H_{12}\left(\frac{\partial\theta_y}{\partial y}+\frac{\partial^2 w_o}{\partial y^2}\right)\Bigg]\frac{1}{h^2}=0 \tag{56}$$

are written as

$$\sum_{j=1}^{N}\alpha_j^{u_o}g_j=0 \tag{57}$$
$$\sum_{j=1}^{N}\alpha_j^{v_o}g_j=0 \tag{58}$$
$$\sum_{j=1}^{N}\alpha_j^{w_o}g_j=0 \tag{59}$$
$$\sum_{j=1}^{N}\alpha_j^{u_o}\left[A_{11}\frac{\partial g_j}{\partial x}\right]+\sum_{j=1}^{N}\alpha_j^{v_o}\left[A_{12}\frac{\partial g_j}{\partial y}\right]$$
$$+\sum_{j=1}^{N}\alpha_j^{w_o}\left[-\frac{4}{3h^2}E_{11}\frac{\partial^2 g_j}{\partial x^2}-\frac{4}{3h^2}E_{12}\frac{\partial^2 g_j}{\partial y^2}\right]$$
$$+\sum_{j=1}^{N}\alpha_j^{\theta_x}\left[B_{11}\frac{\partial g_j}{\partial x}-\frac{4}{3h^2}E_{11}\frac{\partial g_j}{\partial x}\right]$$
$$+\sum_{j=1}^{N}\alpha_j^{\theta_y}\left[B_{12}\frac{\partial g_j}{\partial y}-\frac{4}{3h^2}E_{12}\frac{\partial g_j}{\partial y}\right]=0 \tag{60}$$
$$\sum_{j=1}^{N}\alpha_j^{u_o}\left[\left(B_{11}-\frac{4}{3h^2}E_{11}\right)\frac{\partial g_j}{\partial x}\right]$$
$$+\sum_{j=1}^{N}\alpha_j^{v_o}\left[\left(B_{12}-\frac{4}{3h^2}E_{12}\right)\frac{\partial g_j}{\partial y}\right]$$
$$+\sum_{j=1}^{N}\alpha_j^{w_o}\Bigg[\left(\frac{16}{9h^4}H_{12}-\frac{4}{3h^2}F_{12}\right)\frac{\partial^2 g_j}{\partial y^2}$$
$$+\left(\frac{16}{9h^4}H_{11}-\frac{4}{3h^2}F_{11}\right)\frac{\partial^2 g_j}{\partial x^2}\Bigg]$$
$$+\sum_{j=1}^{N}\alpha_j^{\theta_x}\left[\left(D_{11}-\frac{8}{3h^2}F_{11}+\frac{16}{9h^4}H_{11}\right)\frac{\partial g_j}{\partial x}\right]$$
$$+\sum_{j=1}^{N}\alpha_j^{\theta_y}\left[\left(D_{12}-\frac{8}{3h^2}F_{12}+\frac{16}{9h^4}H_{12}\right)\frac{\partial g_j}{\partial y}\right]=0 \tag{61}$$

The algebraic Eqs. (46)–(60) are solved simultaneously for the unknown α's.

TABLE 1
Comparison of the centroidal deflection of a simply supported square FGM1 plate of aspect ratio $a/h = 20$

	Non-dimensional centroidal deflection				
			Optimal c		
Exponent p	$c = 2/\sqrt{N_a}$; $N_a = 11$ [53]	MLPG code of Qian, Batra & Chen [51]	Present (9×9) grid	Present (11×11) grid	Present (15×15) grid
0	0.02050	0.02118	0.0200	0.0204	0.0207
0.5	0.02760	—	0.0268	0.0274	0.0270
1.0	0.03050	0.03150	0.0297	0.0305	0.0308
2.0	0.03300	0.03395	0.0321	0.0328	0.0338
Metal	0.04430	0.04580	0.0432	0.0442	0.0447

TABLE 2
Comparison of the centroidal deflection of simply supported square FGM1 and FGM2 plates, for $a/h = 5$

(a) FGM1

	Non-dimensional centroidal deflection				
			Optimal c		
Exponent p	$c = 2/\sqrt{N_a}$; $N_a = 11$ [53]	MLPG code of Qian, Batra & Chen [51]	Present (9×9) grid	Present (11×11) grid	Present (15×15) grid
0.0	0.02477	0.02436	0.0243	0.0247	0.0248
0.5	0.03293	—	0.0323	0.0328	0.0330
1.0	0.03666	0.03634	0.0360	0.0365	0.0368
2.0	0.04009	0.03976	0.0394	0.0400	0.0402
Metal	0.05343	0.05253	0.0524	0.0531	0.0536

(b) FGM2

0.0	0.00909	0.00902	0.00891	0.00905	0.00901
0.5	0.01871	—	0.01835	0.01858	0.01876
1.0	0.02381	0.02391	0.02336	0.02370	0.02387
2.0	0.02903	0.02918	0.02847	0.02892	0.02910
Metal	0.05343	0.05253	0.05245	0.05313	0.05358

TABLE 3
Comparison of the centroidal deflection of a simply supported square FGM1 plate

	MLPG [51], 8×8 grid				[53], $c = 2/\sqrt{N_a}$; $N_a = 15$				Optimal c; (15×15) grid			
a/h	$p = 0$	$p = 1.0$	$p = 2.0$	Metal	$p = 0$	$p = 1.0$	$p = 2.0$	metal	$p = 0$	$p = 1.0$	$p = 2.0$	Metal
5	0.02436	0.03634	0.03976	0.05252	0.02476	0.03666	0.04009	0.05342	0.02469	0.03651	0.03998	0.05313
15	0.02115	0.03152	0.03401	0.04583	0.02090	0.03103	0.03354	0.04510	0.02069	0.03075	0.03323	0.04479
25	0.02123	0.03158	0.03404	0.04569	0.02062	0.03061	0.03305	0.04448	0.02030	0.03013	0.03267	0.04388
45	0.02158	0.03203	0.03456	0.04655	0.02057	0.03054	0.03295	0.04437	0.02007	0.02993	0.03293	0.04351
75	0.02190	0.03252	0.03501	0.04728	0.02062	0.03061	0.03302	0.04448	0.01981	0.02938	0.03173	0.04292
125	0.02225	0.03304	0.03562	0.04802	0.02069	0.03072	0.03314	0.04464	0.01959	0.02922	0.03144	0.04270

TABLE 4
Comparison of stress σ_{xx} at the centroids of the top and the bottom surfaces of a simply supported square FGM1 plate

		MLPG [51], 8×8 grid		[53], $c = 2/\sqrt{N_a}$; $N_a = 15$		Optimal c; (15×15) grid	
Exponent p	a/h	$\sigma_{xx}(-h/2)$	$\sigma_{xx}(h/2)$	$\sigma_{xx}(-h/2)$	$\sigma_{xx}(h/2)$	$\sigma_{xx}(-h/2)$	$\sigma_{xx}(h/2)$
0 (ceramic)	20	0.29175	−0.29200	0.28650	−0.28650	0.28648	−0.28648
1	20	0.22617	−0.37875	0.17815	−0.38428	0.22232	−0.37186
2	20	0.24497	−0.40650	0.21278	−0.45899	0.24111	−0.39955
∞ (metal)	20	0.29175	−0.29200	0.28650	−0.28650	0.28648	−0.28648
1	5	0.22540	−0.38812	0.20232	−0.43643	0.22788	−0.38349
1	10	0.22420	−0.37760	0.19812	−0.42737	0.22362	−0.37447
1	15	0.22502	−0.37742	0.19738	−0.42577	0.22255	−0.37236
1	20	0.22617	−0.37875	0.19719	−0.42537	0.22232	−0.37186
1	200	0.23310	−0.38980	0.19841	−0.42800	0.22058	−0.36882

6. COMPUTATION AND DISCUSSION OF RESULTS

Results for a simply-supported FG square plate comprised of aluminum/ceramic, referred to as FGM1, and for an aluminum/silicon carbide square plate referred to as FGM2, are presented in Tables 1–4. Values of material properties of constituents of FGM1 and FGM2 are listed below.

FGM1: $E_1 = 70$ GPa, $\nu_1 = 0.3$; $E_2 = 151$ GPa, $\nu_2 = 0.3$
FGM2: $E_1 = 70$ GPa, $\nu_1 = 0.3$; $E_2 = 427$ GPa, $\nu_2 = 0.17$

In the Tables and Figures to follow, the vertical or the transverse displacement w, the axial stress σ_{xx}, the thickness coordinate z, and the pressure q applied on the top surface of the plate have been non-dimensionalized as follows:

$$\bar{w} = w/h,\ \bar{\sigma}_{xx} = \sigma_{xx}/q,\ \bar{q} = q/E_1 h^4,\ \bar{z} = z/h$$

Henceforth the superimposed bar has been dropped for simplicity. We employ multiquadrics RBFs defined by Eq. (2) with a $N_a \times N_a$ regular grid where N_a is the number of collocation points in either the $x-$ or the y-direction.

Computed results are compared with those obtained by Qian et al. [51] who employed a meshless local Petrov-Galerkin (MLPG) formulation and a 5th order shear and normal deformation theory of Batra and Vidoli [52], and also with those of [53] in which a formulation similar to present formulation is used but without optimizing the shape parameter c in the RBFs. In that case, $c = 2/\sqrt{N_a}$ was chosen, and it gave acceptable results. In all cases, a uniform load parameter, $q = 1$ is applied. We note that Gilhooley et al. [54] have used the RBFs, the MLPG formulation, and the Kth order shear and normal deformable plate theory [52] to analyze deformations of a thick FG plate.

For $N_a = 9, 11$ and 15, we have compared in Table 1 the centroidal deflection of the simply supported square FGM1 plate. For $p = 0, 0.5, 1.0, 2.0$ and ∞, the centroidal deflection computed with $c = 2/\sqrt{11}$ is close to that computed with the present formulation. The same is observed in Tables 2 and 3.

For different values of the index p and the aspect ratio a/h, Table 4 compares the axial stress, σ_{xx}, at centroids of the top and the bottom surfaces of the simply supported square FGM1 plate. Here, the use of the optimization technique improves results, in some cases by 8%, when compared to those of [53].

Figure 1 shows the deformed shape of the plate for 15×15 nodes, $a/h = 20, p = 1$. Figure 2 exhibits through-the-thickness variation of the non-dimensional axial stress σ_{xx}. Except for very large or very small values of p, the axial stress varies smoothly through the plate thickness.

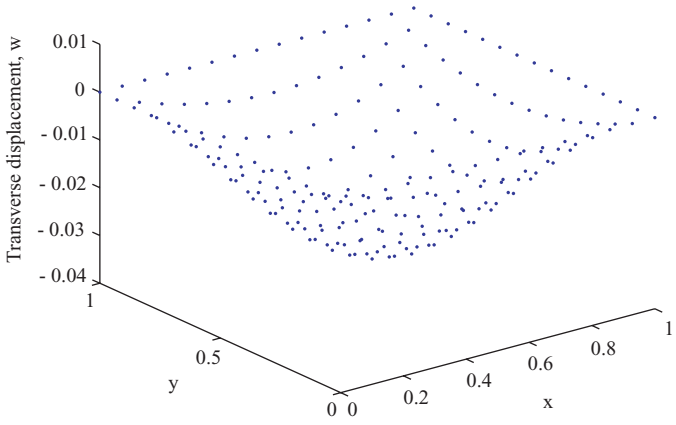

FIG. 1. Non-dimensional deflection, w, for FGM 1 plate, with $N = 15, a/h = 20, p = 1$.

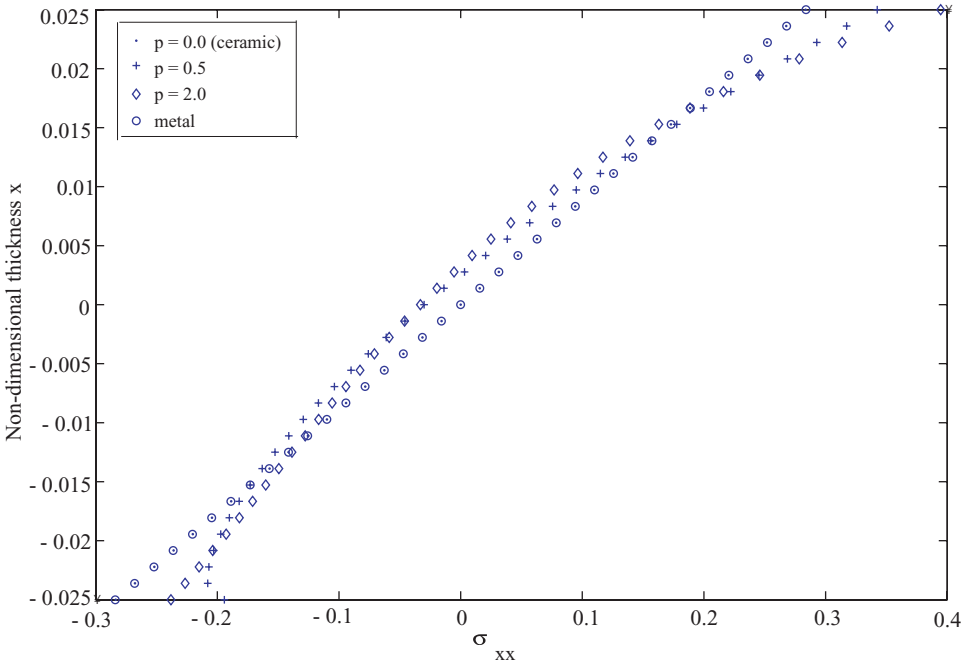

FIG. 2. Through-the-thickness variation of the non-dimensional axial stress for FGM 1 plate with $N = 11$, $a/h = 20$

7. CONCLUSIONS

We have used the meshless collocation method employing multiquadrics basis functions and a third-order shear deformation theory to analyze static deformations of a simply supported square functionally graded plate with the volume fraction of constituents varying only in the thickness direction. A unique feature of the analysis is that it adaptively finds the optimum value of the shape parameter appearing in expressions of the basis functions. Effective material properties are derived by using the Mori-Tanaka homogenization technique. Computed results are found to match well with those obtained from other analyses. The collocation method is truly meshless and neither requires a mesh nor a numerical evaluation of domain integrals, and may be computationally less expensive than other meshless methods.

REFERENCES

1. Hardy, R. L., "Multiquadric equations of topography and other irregular surfaces," *Geophys. Res.* **176**, 1905–1915 (1971).
2. Hardy, R. L., "Theory and applications of the multiquadric-biharmonic method: 20 years of discovery," *Computers Math. Applic.* **19**(8/9), 163–208 (1990).
3. Kansa, E. J., "Multiquadrics- a scattered data approximation scheme with applications to computational fluid dynamics. i: Surface approximations and partial derivative estimates," *Comput. Math. Appl.* **19**(8/9), 127–145 (1990).
4. Kansa, E. J., "Multiquadrics- a scattered data approximation scheme with applications to computational fluid dynamics. ii: Solutions to parabolic, hyperbolic and elliptic partial differential equations," *Comput. Math. Appl.* **19**(8/9), 147–161 (1990).
5. Liu, G. R., *Mesh Free Methods*. CRC Press, Boca Raton, USA (2003).
6. Fasshauer, G. E., "Solving partial differential equations by collocation with radial basis functions," *Surface fitting and multiresolution methods, Vol. 2 Proceedings of the 3rd International Conference on curves and surfaces* **2**, 131–138 (1997).
7. Powell, M. J. D., "The theory of radial basis function approximation in 1990," In F. W. Light, editor, *Advances in Numerical Analysis*, pages 203–240. Oxford University Press (1992).
8. Wendland, H., "Error estimates for interpolation by compactly supported radial basis functions of minimal degree," *J. Approx. Theory* **93**, 258–296 (1998).
9. Wendland, H., *Scattered Data Approximation*. Cambridge University Press, Cambridge, 2005.
10. Hon, Y. C., Lu, M. W., Xue, W. M., and Zhu, Y. M., "Multiquadric method for the numerical solution of byphasic mixture model," *Appl. Math Comput.* **88**, 153–175 (1997).
11. Hon, Y. C., Cheung, K. F., Mao, X. Z., and Kansa, E. J., "A multiquadric solution for the shallow water equation," *ASCE J. Hydraulic Engineering* **125**(5), 524–533 (1999).
12. Wang, J. G., Liu, G. R., and Lin, P., "Numerical analysis of xbiot's consolidation process by radial point interpolation method," *Int. J. Solids and Structures* **39**(6), 1557–1573 (2002).
13. Choy, K.-L., and Felix, E., "Functionally graded diamond-like carbon coatings on metallic substrates," *Materials Science and Engineering A* **278**, 162–169 (2000).
14. Khor, K. A., and Gu, Y. W., "Effects of residual stress on the performance of plasma sprayed functionally graded zro2/nicocraly coatings," *Materials Science and Engineering A* **277**, 64–76 (2000).
15. Reddy, J. N., "Analysis of functionally graded plates," *International Journal for Numerical Methods in Engineering* **47**, 663–684 (2000).
16. Cheng, Z. Q. and Batra, R. C., "Deflection relationships between the homogeneous kirchhoff plate theory and different functionally graded plate theories," *Archive of Mechanics* **52**, 143–158 (2000).
17. Cheng, Z. Q. and Batra, R. C., "Exact correspondence between eigenvalues of membranes and functionally graded simply supported polygonal plates," *Journal of Sound and Vibration* **229**, 879–895 (2000).

18. Cheng, Z. Q. and Batra, R. C., "Three-dimensional thermoelastic deformations of a functionally graded-elliptic plate," *Composites: Part B* **31**, 97–106 (2000).
19. Loy, C. T., Reddy, J. N., and Lam, K. Y., "Vibration of functionally graded cylindrical shells," *International Journal of Mechanical Sciences* **41**, 309–324 (1999).
20. Vel, S. S., and Batra, R. C., "Three-dimensional analysis of transient thermal stresses in functionally-graded plates," *International Journal of Solids and Structures* **40**, 7187–7196, (2004).
21. Vel, S. S., and Batra, R. C., "Three-dimensional exact solution for the vibration of functionally graded rectangular plates," *Journal of Sound and Vibration* **272**, 703–730 (2004).
22. Jin, Z. H., and Batra, R. C., "Some basic fracture mechanics concepts in functionally graded materials," *Journal of the Mechanics and Physics of Solids* **44**, 1221–1235 (1996).
23. Jin, Z. H., and Batra, R. C., "Stress intensity relaxation at the tip of an edge crack in a functionally graded material subjected to a thermal shock," *Journal of Thermal Stresses* **19**, 317–339 (1996).
24. Jin, Z. H., and Batra, R. C. "R-curve and strength behavior of a functionally gradient material," *Material Science & Engineering*, A2 **42**, 70–76 (1998).
25. Vel, S. S., and Batra, R. C., "Exact solution for thermoelastic deformations of functionally graded thick rectangular plates," *AIAA Journal* **40**, 1421–1433 (2002).
26. Fedoseyev, A. I., Friedman, M. J., and Kansa, E. J., "Continuation for nonlinear elliptic partial differential equations discretized by the multiquadric method," *Comput. Math. Appl.* **19**(8/9), 147–161 (1990).
27. Hon, Y. C., and Mao, X. Z., "On unsymmetric collocation by radial basis functions," *Appl. Math. Comput.* **119**(2–3), 177–186 (2001).
28. Kansa, E. J., and Hon, Y. C., "Circunvecting the ill-conditioning problem with multiquadric radial basis functions," *Comput. Math. Appl.* **39**(7–8), 123–137 (2000).
29. Belytschko, T., Krongauz, Y., Organ, D., Fleming, M., and Krysl, P., "Meshless methods: an overview and recent developments," *Comp. Meth. in Appl. Mech. and Eng.* **139**, 3–47 (1996).
30. Belytschko, T., Lu, Y. Y., and Gu, L., "Element free galerkin methods," *Int. J. Num. Meth. Eng.* **37**, 229–256 (1994).
31. Duarte, C. A., and Oden, J. T., "An hp adaptive method using clouds," *Comp. Meth. in Appl. Mech. and Eng.* **139**, 237–262 (1996).
32. Nayroles, B., Touzot, G., and Villon, P., "Generalizing the finite element method: diffuse approximation and diffuse elements," *Comp. Mechanics* **10**, 307–318 (1992).
33. Melenk, J. M., and Babuska, I., "The partition of the unity finite element method," *Computer Methods in Applied Mechanics and Engineering* **139**, 289–314 (1996).
34. Sukumar, N., Moran, B., and Belytschko, T., "The natural element method in solid mechanics," *International Journal for Numerical Methods in Engineering* **43**, 839–887 (1998).
35. Atluri, S. N., and Shen, S. P., *The meshless local Petrov-Galerkin (MLPG) method*. Tech. Science Press (2002).
36. Atluri, S. N., and Zhu, T., "A new meshless local petrov-galerkin (mlpg) approach in computational mechanics," *Computational Mechanics* **22**, 117–127 (1998).
37. Ferreira, A. J. M., "A formulation of the multiquadric radial basis function method for the analysis of laminated composite plates," *Composite Structures* **59**, 385–392 (2003).
38. Ferreira, A. J. M., "Thick composite beam analysis using a global meshless approximation based on radial basis functions," *Mechanics of Advanced Materials and Structures* **10**, 271–284 (2003).
39. Rippa, S., "An algorithm for selecting a good value for the parameter *c* in radial basis function interpolation," *Advances in Computational Mathematics* **11**, 193–210 (1999).
40. Zienkiewicz, O. C., *The finite element method*. McGraw-Hill (1991).
41. Hughes, T. J. R., *The finite element method-Linear static and dynamic finite element analysis*. Dover Publications, New York (2000).
42. Bathe, K. J., *Finite element procedures in engineering analysis*. Prentice Hall (1982).
43. Beatson, R. K., "Fast fitting of radial basis functions: Methods based on preconditioned gmres iteration," *Adv. in Comput. Math.* **11**, 253–270 (1999).
44. Hon, Y. C., and Schaback, R., "On unsymmetric collocation by radial basis functions," *Appl. Math. Comput.* **119**, 177–186 (2001).
45. Wang, B. P., "Parameter optimization in multiquadric response surface approximations," *Structural and Multidisciplinary Optimization* **26**, 219–223 (2004).
46. Schaback, R., and Wendland, H., "Adaptive greedy techniques for approximate solution of large rbf systems," *Numer. Algorithms* **24**, 239–254 (2000).
47. Hon, Y. C., Schaback, R., and Zhou, X., "An adaptive greedy algorithm for solving large rbf collocation problems," *Numer. Algorithms* **73**, 13–25 (2003).
48. Cheng, A. H.-D., Golberg, M. A., Kansa, E. J., and Zammito, G., "Exponential convergence and h-c multiquadric collocation method for partial differential equations," *Numer Methods Partial Differential Eq* **19**, 571–594 (2003).
49. Reddy, J. N., "A simple higher-order theory for laminated composite plates," *Journal of Applied Mechanics* **51**, 745–752 (1984).
50. Reddy, J. N., *Mechanics of laminated composite plates*. CRC Press, New York (1997).
51. Qian, L. F., Batra, R. C., and Chen, L. M., "Static and dynamic deformations of thick functionaally graded elastic plate by using higher-order shear and normal deformable plate theory and meshless local Petrov-Galerkin method," *Composites Part B* **35**(6–8), 685–697 (2004).
52. Batra, R. C., and Vidoili, S., "Higher order piezoelectric plate theory derived from a three-dimensional variational principle," *AIAA Journal* **40**(1), 91–104 (2002).
53. Ferreira, A. J. M., Batra, R. C., Roque, C. M. C., Qian, L. F., and Martins, P. A. L. S., "Static analysis of functionally graded plates using third-order shear deformation theory and a meshless method," *Composite Structures* **69**, 449–457 (2005).
54. Gilhooley, D. F., Batra, R. C., McCarthy, J. R., Xiao, M. A., and Gillespie Jr., J. W., "Analysis of thick functionally graded plates by using higher-order shear and normal deformable plate theory and mlpg method with radial basis functions," *Composite Structures*, **80**, 539–552 (2007).